Article

pubs.acs.org/Biomac

Photosensitive Peptidomimetic for Light-Controlled, Reversible DNA Compaction

Selina Schimka,[†,‡] Svetlana Santer,[*,†] Nina M. Mujkić-Ninnemann,[‡] David Bléger,[§] Laura Hartmann,[*,‡,∥] Marko Wehle,[⊥] Reinhard Lipowsky,[⊥] and Mark Santer[*,⊥]

[†]Institute of Physics and Astronomy, University of Potsdam, 14476 Potsdam, Germany

[‡]Max Planck Institute of Colloids and Interfaces, 14424 Potsdam, Germany

[§]Humboldt-Universität zu Berlin, 12489 Berlin, Germany

[⊥]Theory and Bio-Systems Group, Max Planck Institute of Colloids and Interfaces, 14424 Potsdam, Germany

Supporting Information

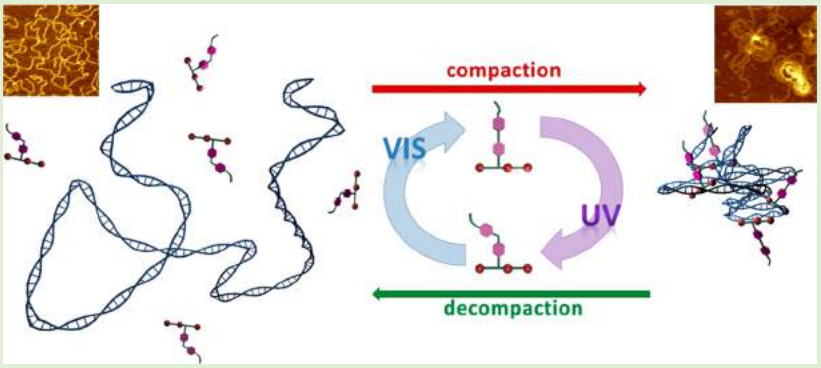

ABSTRACT: Light-induced DNA compaction as part of nonviral gene delivery was investigated intensively in the past years, although the bridging between the artificial light switchable compacting agents and biocompatible light insensitive compacting agents was not achieved until now. In this paper, we report on light-induced compaction and decompaction of DNA molecules in the presence of a new type of agent, a multivalent cationic peptidomimetic molecule containing a photosensitive Azo-group as a branch (Azo-PM). Azo-PM is synthesized using a solid-phase procedure during which an azobenzene unit is attached as a side chain to an oligo(amidoamine) backbone. We show that within a certain range of concentrations and under illumination with light of appropriate wavelengths, these cationic molecules induce reversible DNA compaction/decompaction by photoisomerization of the incorporated azobenzene unit between a hydrophobic *trans*- and a hydrophilic *cis*-conformation, as characterized by dynamic light scattering and AFM measurements. In contrast to other molecular species used for invasive DNA compaction, such as widely used azobenzene containing cationic surfactant (Azo-TAB, C_4-Azo-OC_X-TMAB), the presented peptidomimetic agent appears to lead to different complexation/compaction mechanisms. An investigation of Azo-PM in close proximity to a DNA segment by means of a molecular dynamics simulation sustains a picture in which Azo-PM acts as a multivalent counterion, with its rather large cationic oligo(amidoamine) backbone dominating the interaction with the double helix, fine-tuned or assisted by the presence and isomerization state of the Azo-moiety. However, due to its peptidomimetic backbone, Azo-PM should be far less toxic than photosensitive surfactants and might represent a starting point for a conscious design of photoswitchable, biocompatible vectors for gene delivery.

INTRODUCTION

Nature has found clever ways how to store a very long DNA molecule in a compact region of space. For instance, a human chromosome containing one DNA molecule with a length of about several centimeters has a width of no more than 1,5 μm. The mechanisms of DNA compaction are not only interesting from a fundamental point of view, but also inspire the engineering of vectors suitable for gene delivery as part of gene therapy.[1]

Gene delivery is commonly accomplished with suitable viruses, the native DNA of which has partially been replaced with the desired chunks of target DNA. By the natural infection process, the DNA can be transferred into the cell. Although this is by far the most widely used technique, immunological risks remain, and nonviral synthetic approaches to gene delivery are called for.[2] The crucial step is an adequate compaction of the DNA strand to be delivered, from the extended coil conformation to a compacted globular state.[3] Presently there

Received: January 13, 2016
Revised: March 29, 2016
Published: March 31, 2016

DOI: 10.1021/acs.biomac.6b00052
Biomacromolecules 2016, 17, 1959−1968

Scheme 1. Scheme of the Synthesis of the Photosensitive Oligo(amidoamine) Molecules (Azo-PM)

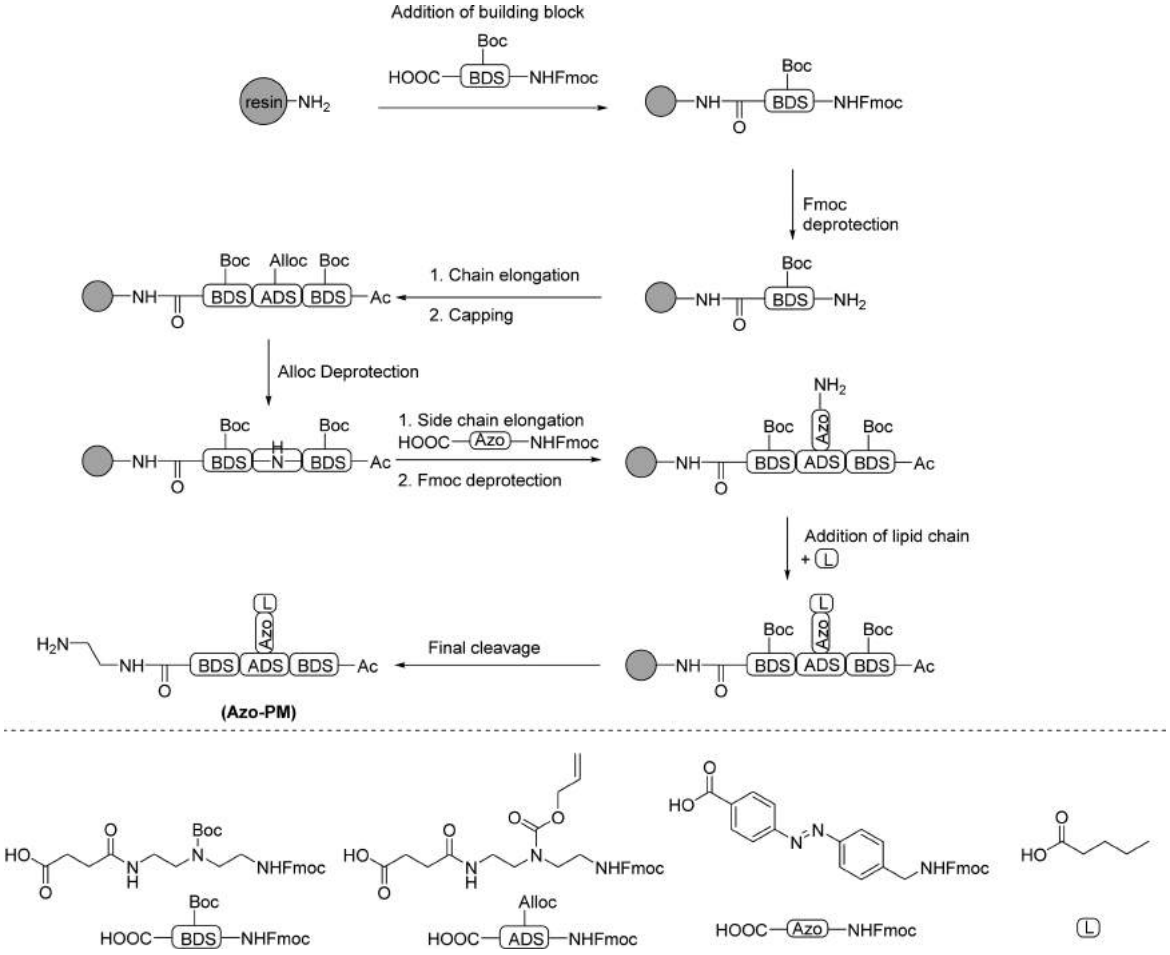

is consensus that compaction of DNA into small particles along with a reduction of its net charges facilitates the uptake by cells through their plasma membrane.[4−7]

There are quite a number of strategies to accomplish DNA compaction by complex formation with other molecular species such as cationic surfactants, polyelectrolytes, multivalent cations, cationic dendrimers, nanoparticles, and polyamines.[8−18] In all of these strategies, decompacting the complex after transfection is the main problem. Indeed, with the existing approaches, once the compacted DNA has been transferred into the cell, it must find suitable conditions such as pH or ionic strength, in order to trigger decompaction.[19,20]

Recently it was proposed to achieve DNA compaction/decompaction employing azobenzene containing cationic surfactant.[21,22] The surfactant consists of one or two charged groups connected to a hydrophobic tail with an azobenzene group incorporated. Under external illumination, the azobenzene undergoes a photoisomerization reaction from the more stable *trans*- to the *cis*-conformation, resulting in a change of surfactant hydrophobicity. The *cis*-isomer, which exhibits a pronounced dipole moment, is more hydrophilic than its *trans* counterpart.[23,24] When the azobenzene containing surfactants are added to the DNA solution, they are thought to associate into aggregates near the polyelectrolyte DNA strand at a critical aggregation concentration and bind cooperatively to the chain (see also the section Discussion and Computational Results). This process results in a pronounced shrinkage of the DNA coil, ultimately leading to a compacted state.[25−29] Decompaction is achieved under irradiation with UV light at which the *trans*-isomers are converted to the *cis*-state and leave the DNA globule. The efficiency by which compaction can be achieved depends on surfactant structure. For example, when the length of the hydrophobic spacer connecting the azobenzene moiety to a charged headgroup increases from 6 to 10 CH_2 groups, the concentration of surfactant needed to trigger compaction decreases almost by a factor of 2.[30−33] The concentration of the compacting agent is a crucial point since less cationic surfactant in solution implies a reduced toxicity, so far a major drawback of this approach for use in in vivo applications. The cationic headgroup of the surfactant is rather toxic in particular. Therefore, an alternative approach would be to use a headgroup based on an oligocation; for instance, oligo(amidoamines) have shown to reduce toxicity while remaining efficient for DNA compaction properties.[17,34]

In this paper, we aim at combining the aspects of photosensitivity and biocompatibility and design a complexing agent by coupling an azobenzene containing, photosensitive lipophilic unit to a multivalent, cationic oligo(amidoamine) backbone. The latter, however, will be much larger in comparison to the hydrophobic, azobenzene containing unit that is attached as a side chain, such that the overall appearance of the azobenzene containing peptidomimetic system (Azo-PM) is rather that of multivalent cation similar to the well-known natural compacting agent spermidine. We report on the synthesis of Azo-PM and demonstrate how compaction of DNA coils can be achieved and that compaction/decompaction

DOI: 10.1021/acs.biomac.6b00052
Biomacromolecules 2016, 17, 1959−1968

Scheme 2. Chemical Structure of the Azobenzene Containing Peptidomimetic Surfactant (Azo-PM), EDA-BDS-ADS(Azo,Pent)-BDS-NHAc in Full Notation[a]

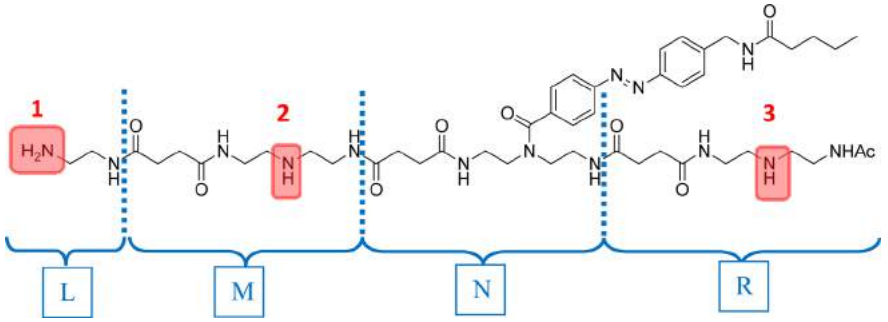

[a]Red shaded amine groups indicate the protonation sites 1−3 of the molecule. The segments L, M, N, and R bounded by the dashed lines correspond to the building blocks used in the synthesis. In the computational model, they are assigned fixed group charges of +1/0 (L, M, and R) and 0 (N), to allow for a modular buildup in the simulation as well.

can be conducted in a reversible manner by light irradiation at two different wavelengths. We employ dynamic light scattering and AFM imaging in order to characterize size and shape changes of the compacted DNA: Supported by atomistic simulations, we can elucidate molecular scale details of the interaction of the Azo-PM molecule with the DNA surface.

EXPERIMENTAL SECTION

Synthesis of Azobenzene Containing Peptidomimetic Surfactant (Azo-PM). *General Methods.* Unless otherwise noted, all solvents used were HPLC grade. The solid-support resin was purchased from Rapp Polymers. Reversed-phase HPLC (RP-HPLC) was performed on Agilent 1200 using an Agilent Zorbax EclipseXDB-C18 (4.6 × 100 mm) column at a flow rate of 1 mL/min at 60 °C. Acetonitrile (MeCN) and water with 0.1% trifluoroacetic acid (TFA) were used as eluents. Compounds were dissolved in water. Preparative HPLC was carried out with a Varian Pursuit 10 μ C18 column (250 × 10 mm) at room temperature with a flow rate of 3 mL/min. The UV signal was detected at 214 nm, fluorescence (Fmoc) was detected at 259 nm (extinction) and 311 nm (emission). The purity was determined by integration of the UV-signal with the software ChemStation for LC from Agilent Technologies.

Materials. The building blocks, Boc-protected ethylendiamine succinic anhydride dimer building block (BDS) and Alloc-protected ethylendiamine succinic anhydride dimer building block (ADS; Scheme 1), were synthesized as described elsewhere.[35] The building block containing the Azo-moiety (Scheme 1), N-Fmoc-*para*-(aminomethyl)phenylazobenzoic acid, was synthesized according to literature.[36,37] Pentanoic acid was purchased from Sigma-Aldrich.

Solid Phase Synthesis. Tentagel S Trityl OH resin (7.5 g, loading 0.25 mmol/g) was washed with DCM, then with dry toluene. The resin beads were covered with dry toluene and freshly distilled acetyl chloride (12 mL) was added and the mixture was refluxed at 60 °C for 3 h. After cooling to room temperature, the resin was washed with toluene. Freshly distilled ethylene diamine EDA (dried over KOH pellets overnight) was added, the reaction mixture was shaken for 48 h, and then the resin was washed with MeOH and DCM. Loading of Tentagel-Trt-EDA resin was determined by standard loading test: Fmoc-Glycin was coupled to the resin, followed by cleavage with 1,8-diazabicyclo[5.4.0]undec-7-en (DBU). The UV absorption of the DBU-Fmoc was measured at 304 nm. Fmoc-loading: mmol/g = $Abs_{sample} - Abs_{ref} \times 6.4$. A loading of 0.23 mmol/g was determined.[38,39,48]

General Coupling Protocol (Scheme 1). Tentagel-Trt-EDA-resin (0.1 mmol, 0.45 g) was swollen in dichloromethane for 20 min, then washed with DCM and DMF. Initial coupling to the EDA linker was performed by dissolving the desired building block BDS or ADS (0.5 mmol, 5 equiv) in DMF (1 mL), followed by the addition of a solution of PyBOP (0.49 mmol, 4.9 equiv) and HOBt (0.49 mmol, 4.9 equiv) in DMF (1 mL). DIPEA (1.6 mmol, 16 equiv) was added, and the mixture was shaken for 30 s, then added to the resin. The reaction mixture was shaken for 1 h. Afterward, the resin was washed 10 times with DMF, and Fmoc deprotection was performed using a solution of 25% piperidine in DMF three times for 10 min. Thereafter, the resin was washed extensively with DMF before repeating the coupling protocol with the next building block.

Capping of N-Terminal Site. After successful assembly of the desired number of building blocks on solid phase, the *N*-terminal site was capped with an acetyl group. Therefore, the resin was washed three times with DCM, then acetic anhydride (10 mL) was added and the mixture was shaken for 15 min. Afterward, the resin was washed with dichloromethane.

Introduction of a Side Chain via Alloc Cleavage. The Alloc protecting group was cleaved by the addition of premixed $Pd(PPh_3)_4$ (0.3 equiv per Alloc moiety) and *N,N*-dimethylbarbituric acid (15 equiv per Alloc moiety) in dry dichloromethane (4 mL) under an argon atmosphere. After 2 h, the resin was washed as follows: chloroform, 10% DIPEA in DCM, DCM, 23 mM sodium dithiocarbamate in DMF, DMF and DCM. The whole washing procedure was repeated three times followed by an additional Alloc cleavage overnight. After successful deprotection of the Alloc protecting group, the side chain was introduced according to the general coupling protocol starting with the Fmoc protected building block containing the Azo-moiety. The coupling reaction was protected from light.

Coupling of Lipid Side Chain. After successful coupling of the Azo building block, Fmoc cleavage in the side chain was performed by standard conditions as described previously. Coupling of the lipid side chain was achieved by activation of pentanoic acid (0.8 mmol, 8 equiv) with PyBOP (0.8 mmol, 8 equiv), HOBt (0.4 mmol, 4 equiv), and DIPEA (0.4 mmol, 4 equiv) in DMF (1 mL) and addition to the resin for 1 h. The resin was washed with DMF and DCM before final cleavage of the product.

Cleavage from Solid Phase. Final cleavage was performed by the addition of 30% TFA in DCM (1 mL/50 mg resin) to the resin and allowing it to react for 1 h. The cleavage solution was filtered and purged into ice-cold diethyl ether. The precipitate was isolated by centrifugation and washed three times with diethyl ether (40 mL each). The residue was dissolved in water (1 mL) and lyophilized overnight, giving the final Azo-PM or EDA-BDS-ADS(Azo,Pent)-BDS-NHAc (Scheme 2).

The compound was synthesized by applying the general coupling protocol three times with building blocks in the sequence BDS, ADS, BDS. After capping the primary amine with acetic anhydride, the Alloc protecting group was cleaved as described and the side chain was introduced via the general coupling protocol two times with building blocks in the sequence Azo, pentanoic acid. The final Azo-PM was cleaved from the resin as the last step and purified by preparative RP-HPLC giving the final product in 23% yield (23 mg, 0.023 mmol).

DOI: 10.1021/acs.biomac.6b00052
Biomacromolecules 2016, 17, 1959−1968

^{1}H NMR (400 MHz, D_2O): δ 7.94 (m 4H, Ar*H*), 7.56 (m, 4H, Ar*H*), 4.49 (s, 2H, Ar-CH_2-), 3.77−3.01 (m, 26H, -NH-CH_2), 2.63−2.24 (m, 16H, C(O)-CH_2), 2.00−1.89 (m, 3H, -C(O)CH_3), 1.65−1.51 (m, 2H, -CH_2-CH$_2$-CH$_3$), 1.34 (m, 2H, -CH$_2$-CH_2-CH$_3$), 0.89 (m, 3H, -CH$_2$-CH_3). RP-HPLC (5−30% MeCN in H_2O in 30 min): t_R = 14.8 min (98% pure). ESI-MS calcd for $C_{47}H_{74}N_{14}O_9$ $[M + H]^+$, 979.58; found, 979.57; $[M + 2H]^{2+}$, 490.29; found, 490.51; $[M + 3H]^{3+}$, 327.20; found, 327.40; $[M + Na]^+$, 1001.57; found, 1001.58.

The ^{1}H NMR, RP-HPLC, and ESI-MS data of the final product can be found in the Supporting Information (Figures S1, S2, and S3, respectively).

Preparation of DNA-Azo-PM Complexes. Calf thymus DNA type I, M_w = 10.8 × 10^6 Da, with 6% sodium salt was purchased from Sigma (D1501). The DNA was diluted in Milli-Q water, filtered, and then spiked with NaCl, to obtain a salt concentration of 5 mM. All experinemts were performed at 5 mM NaCl ionic strength and pH = 6. The Azo-PM is used in a 5 mM NaCl aqueous solution, if not mentioned otherwise. To prepare complexes between Azo-PM and DNA, 5 mM NaCl aqueous solutions of both components at certain concentrations were mixed at room temperature and stored overnight in the fridge before further use. The pH value was kept constant at neutral value. The irradiation of the samples was carried within 10 min to get a steady state of the azobenzenes. AFM samples were then prepared within 1 h and the DLS measurements were carried out within the following 2 h after irradiation. The AFM samples were prepared by spin-casting of a solution on a mica surface at 2000 rpm during 3 min.

Methods. The lamps UV inspector (Göhler HPLC analyses technique, Germany; 365 nm, 1.2 mW/cm^2) and LED Spot Luxeon Royal Blue, P453E-PR09 (Conrad Electronic; 453 nm, 7 mW/cm^2) were used for irradiation of the samples. The irradiation time was fixed at 10 min, to reach so-called steady state, where the rates of *trans*−*cis* and *cis*−*trans* (*Z*−*E*) isomerizations are the same. Under these irradiation conditions the nativity of the DNA molecule does not change. UV−vis spectra of the solutions in quartz cuvettes of 40 mm optical pathway were obtained using Cary 5000 UV−vis-NIR spectrophotometer (Varian, Inc.). The dynamic light scattering (DLS) characterization of the DNA-Azo-PM complexes was performed in micro UV-cuvettes using Zetasizer Nano ZS (Malvern Instruments Ltd.) at a scattering angle of 173°. To acquire the morphology of the DNA-Azo-PM complexes adsorbed on the mica surface, atomic force microscopy (AFM; Nanoscope V, Bruker, U.S.A.) was utilized operating in tapping mode, with commercial tips (NanoSensors) of a resonance frequency 320 kHz, and a spring constant of ∼42 N/m. The AFM micrographs were recorded in air at a temperature of 23 °C and overall humidity of 55%. All experiments were carried out in a room with yellow light to avoid any premature isomerization of the azobenzene.

Computational Methods. For all quantum-chemical calculations we used Gaussian03,[40] the development of the Azo-PM model was conducted mainly with the Amber 14 suite of programs,[41] including Amber Tools 14, Antechamber, and tleaP. Parameters for the DNA strand were taken from the ff99SB force field.[42] This is an updated version of the Parm99 force field used by Savelyev and Papoian in their study of counterion condensation on the DNA double helix, with the same LJ parameters for all atom types. These parameters are compatible to those used in the General Amber Force Field (GAFF),[43] which was employed to model the Azo-PM molecules. Parameters for bonded interaction for the azo moiety were taken from Duchstein et al.[44] Partial charges for Azo-PM were derived by employing the standard 2-stage Amber protocol with electronic charge densities computed at the HF/6-31G* level of theory. As the full Azo-PM molecule is expected to be quite flexible, atomic partial charges were assigned by defining fixed net charges (group charges) on segments corresponding to the chemical building blocks, see Scheme 2. These are 0 for N and either +1 or 0 for L, M, and R, depending on the protonation state. For each segment, partial charges are then determined by two stages of averaging. In addition to the full Azo-PM structure Scheme 2, we also consider smaller molecular fragments that contain fewer segments, duly capped with corresponding amine- or O-acetyl groups. For instance, to set the charges on L, we considered capped fragments consisting of L, L + M, and L + M + N, and the final charges on L were determined as the average over the fragments, in order to reflect the molecular context. Each of the fragments subjected to an ensemble average (EA) procedure, originally suggested for carboyhdrates.[45] Starting with a preliminary set of charges according to the semiempirical theory level AM1 including a bond charge correction (AM1BCC),[46] a 50 ns MD run with explicit solvation using the TIP3P water model is performed. From this run, the charge set on the fragment is calculated as the average of 200 snapshots along the trajectory according to the standard Amber 2-stage protocol. The final charge set is then taken as the arithmetic average, restraints on group charges enabled. For segment N, a distinction is made between the *cis* and the *trans* isomers of the azobenzene unit, each acquiring slightly different sets of partial charges reflecting the pronounced change in dipole moment upon isomerization in a better way. The whole procedure renders the organization of the parameter set modular, and in principle larger polymers of the elementary Azo-PM unit can be assembled. Production runs were carried out with GROMACS 4.5.5[47] using a time step of 2 fs and a Langevin-type thermostat in TIP3P water at 300 K. Each simulation was carried out for 200 ns with trajectory snapshots output every 10 ps (20.000 per trajectory). Translation of Amber into GROMACS force field topology files was carried out using an adapted version of the amb2gmx.pl script.[48]

EXPERIMENTAL RESULTS

The synthesis of the Azo-PM was conducted following the solid phase polymer synthesis of poly(amidoamines) as described elsewhere.[49]

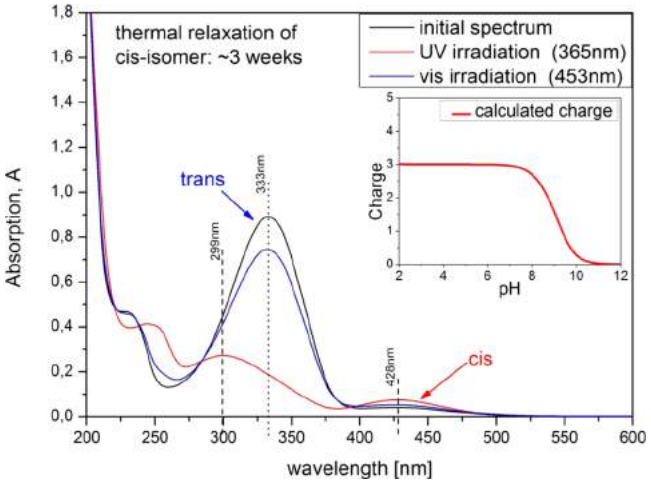

Figure 1. UV−vis absorption spectra of Azo-PM in water. Black: *trans*-isomer in the initial dark state; Red: *cis*-isomer after irradiation with UV light at 365 nm; Blue: *trans*-isomer after subsequent irradiation with blue light at 453 nm. Irradiation time for both events is 10 min. Inset shows the dependence of the Azo-PM molecule charge on pH as calculated from the Henderson−Hasselbach equation and local amine-pK_a values determined using Marvin Sketch.[53]

The Azo-PM consists of three parts, the cationic oligo(amidoamine) backbone and a short lipid tail attached to an azobenzene side chain. All three parts are assembled through the stepwise addition of functional building blocks on solid support using standard peptide coupling chemistry (Scheme 1). First, the oligo(amidoamine) backbone is built up introducing temporarily Boc and Alloc protected amine groups in the main chain. In a second step, the Alloc protection groups are selectively cleaved off on solid support releasing a single secondary amine group within the oligo(amidoamine) backbone. This is used as an anchoring point to attach the azobenzene side chain. In the final step, the side chain is elongated by coupling with pentanoic

DOI: 10.1021/acs.biomac.6b00052
Biomacromolecules 2016, 17, 1959−1968

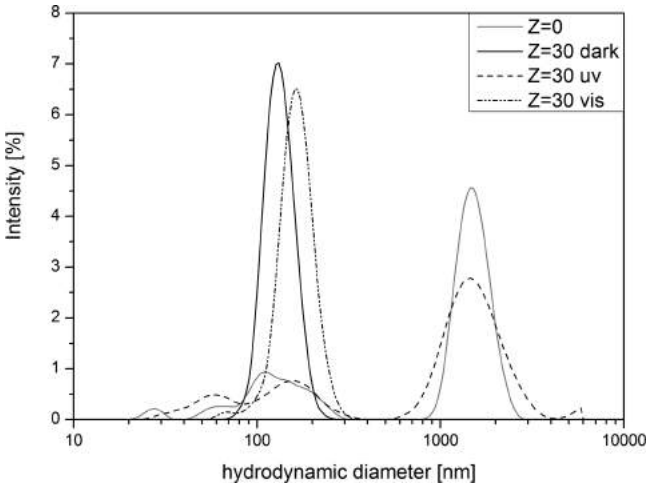

Figure 2. DLS data of DNA (Z = 0, gray curve) and the DNA/Azo-PM complex at Z = 30 prepared in dark (black curve), irradiated with UV light (dotted line), and subsequent irradiation with blue light (dotted-dashed line).

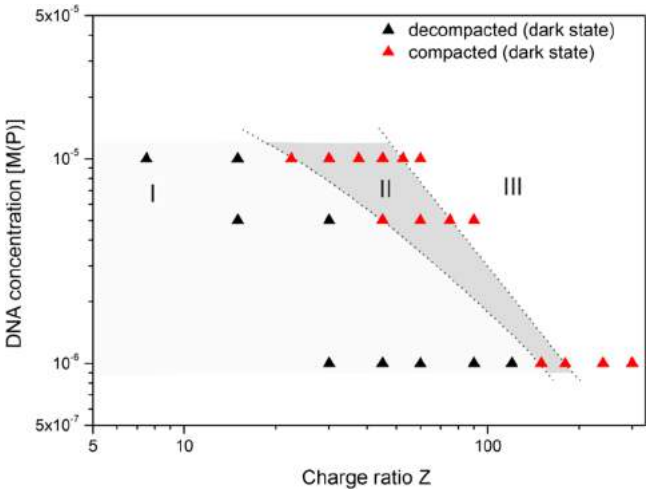

Figure 3. Phase diagram of DNA compaction and decompaction with different DNA concentrations.

acid, introducing a short lipid tail, followed by cleavage and purification of the desired Azo-PM.

The oligo(amidoamine) backbone (Scheme 2) of Azo-PM can carry up to three charges, depending on the pH value. For instance, at pH between 2 and 7, all three amine groups (marked in red in Scheme 2) are protonated. The pH dependence of the protonation state was calculated using a standard procedure as part of a commercially available program (Marvin Sketch; inset in Figure 1). In the present study, the pH is kept constant at a value of 6, resulting in three positively charged sites 1−3 (Scheme 2) at infinite dilution. We should mention that the pK_a of related polyamines such as spermidine or spermine, for instance, depends only mildly on ionic strength and even slightly increases with molar concentration.[50] For other polyamines, such as the well-known spermidine, full protonation is usually assumed under physiological conditions in simulations and in interpreting experimental data.[51,62,62] According to distance measurements in linearly extended Azo-PM molecules subject to preliminary molecular-mechanical relaxation with a classical force field using Avogadro,[52] the charges along the backbone are 1.4 nm (first and second amine, Scheme 2) and 2.7 nm apart, respectively (second and third amine, Scheme 2), while the photosensitive side chain is at equal distances from the second and third amine groups.

The photoisomerization process of the Azo-PM was monitored by UV−vis spectroscopy (Figure 1). In the nonirradiated "dark state", where almost all molecules are in the *trans* state, the spectra show a main peak at 333 nm corresponding to an absorption band of the $\pi-\pi^*$ transition. The band with a maximum at 240 nm corresponds to the absorption of the π-conjugated benzene rings present in both isomers. After irradiation with UV light (λ = 365 nm), the majority of azobenzene moieties isomerizes into the *cis*-state, which is characterized by two absorption bands with maxima at 299 nm ($\pi-\pi^*$ transition) and 428 nm ($n-\pi^*$ transition). Irradiation with visible light at 453 nm induces isomerization back to the *trans* conformation (Figure 1). However, the irradiation does not lead to a complete return to the initial dark state: only 83% of the initial *trans* isomers are formed.

To estimate the amount of *trans* isomers in solution under the photoisomerization process, we utilize the absorption at 352 nm, where the absorption of the *cis* isomer is minimal, and find that 83 and 17% of the molecules are in the *trans* state under visible and UV irradiation, respectively. The typical amount of *cis* azobenzene groups produced is comparable to other azobenzene containing compaction agents.[30] The spectra after irradiation for 10 min correspond to the so-called steady state when further irradiation does not lead to spectral changes due to equal rates of forward and backward isomerizations. The discrepancy between spectra acquired in the dark and under irradiation with blue light can be explained by the simultaneous absorption of blue light by both, *cis* and *trans* isomers, preventing full recovery of the "dark state". Thermal *cis*−*trans* isomerization takes more than 3 weeks. The lifetime of the *cis*-isomer was measured spectroscopically, as shown in the Supporting Information, Figure S4. Because of the long lifetime, the spectra do not notably change after the irradiation is turned off. Concluding, the surfactant in the "dark state" should never be thought of as being pure *trans*.

The complexes between DNA and Azo-PM were prepared at different charge ratios Z, each sample left overnight for equilibration. The charge ratio is defined as Z = 3 [Azo-PM]/[DNA-nucleotides], which is the molar ratio of charges on all Azo-PM to the total number of DNA phosphate groups (that is, nucleotides). In this work, we chose three concentrations C_{Nuc} (=[DNA − nucleotides], moles of nucleotides per liter): 10^{-5}, 5×10^{-6}, and 10^{-6} M, in order to acquire a phase diagram of DNA compaction. C_{Nuc} thus was far below the overlapping concentration of $\approx 3.3 \times 10^{-4}$ M: with an average number of 16.000 base pairs per DNA strand, we may quote an average concentration of DNA coils as $C_{DNA} = C_{Nuc}/32.000$. This would correspond to one coil per cube of edge length 1.7 μm ($C_{Nuc} = 10^{-5}$), for $C_{Nuc} = 10^{-6}$ M the edge length would be 3.8 μm, respectively. This should be compared to the expected radius of gyration R_g = 300 nm of the average DNA coil.

In order to monitor the expected DNA compaction upon addition of Azo-PM, we first utilize dynamic light scattering. Figure 2 shows the intensity distribution of the effective hydrodynamic diameter of aggregates of Azo-PM/DNA complexes at different Z ratios. At first, DNA without any compacting agent was measured to obtain a size reference for uncompacted DNA. The built-in modeling software (DTS Nano, Dispersion Technology Software, v.5.10, Malvern Instruments Ltd.) generated from DLS measurements the multimodal size distributions typical for the extended, coiled DNA (Z = 0.0). The broadening of the peaks around 140 and 1500 nm can be related to diffusion, rotation, or internal translation modes. Although the distribution does not rigorously describe the state of extended coil DNA in solution, it can be considered as a "fingerprint" of the used DNA.[54−56] This distribution changes considerably when Azo-PM is added to the DNA solution starting from a certain value of Z.

Thus, for C_{Nuc} of 10^{-5} M, a sharp peak at 130 nm occurs, indicating the compacted state that is observed from Z = 22.5 onward. The onset of compaction shifts toward Z = 45 and 150 for decreasing C_{Nuc} of 5×10^{-6} M and 10^{-6} M, respectively (see Figure 3). Figure 2 shows the curves only for the value Z = 30.0, where the compaction is present, for other Z value DLS data are presented in the Supporting Information, Figure S5.

DOI: 10.1021/acs.biomac.6b00052
Biomacromolecules 2016, 17, 1959−1968

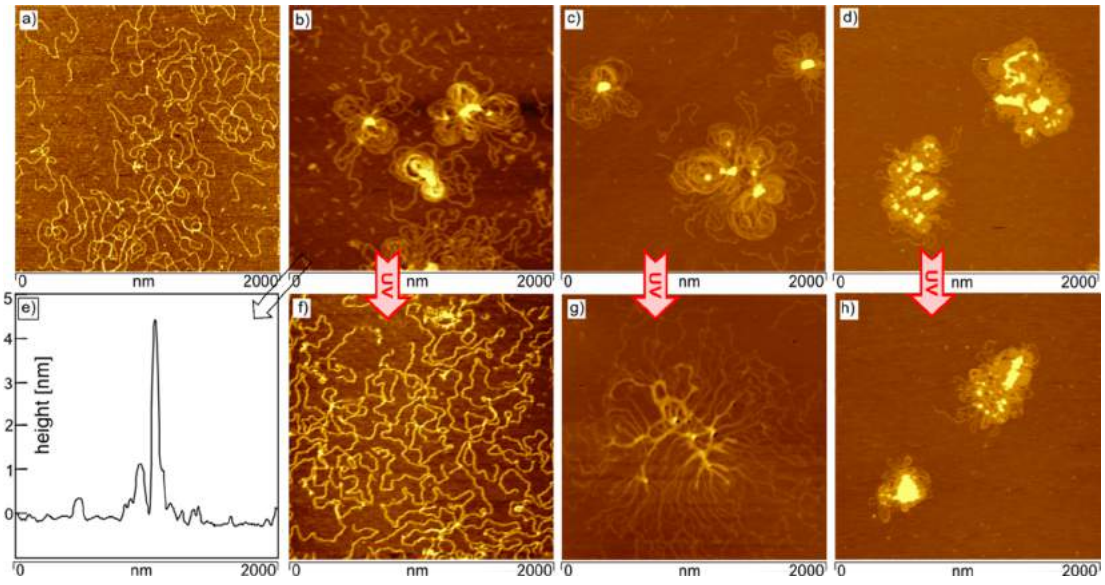

Figure 4. AFM mircographs of the DNA/Azo-PM complex prepared in dark at different Z values: (a) $Z = 0$, (b) $Z = 30$, (c) $Z = 60$, and (d) $Z > 100$. The DNA concentration is fixed at 1×10^{-5} M (ionic strength is 5 mM NaCl, pH = 6). (f–h) Corresponding DNA/Azo-PM complexes after irradiation with UV light (λ = 365 nm, I = 5 J/cm^2). A height profile for a DNA/Azo-PM complex from picture (b) is shown in (e).

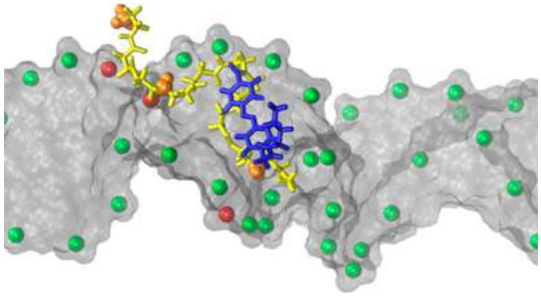

Figure 5. Single Azo-PM molecule in the vicinity of a 64 Å long DNA double strand (gray, horizontal direction is the z-axis): blue, azobenzene and hydrophobic tail; yellow, peptidomimetic backbone; orange, protonated amine groups along the backbone; red, phosphate groups closest (distance < 4 Å) to each protonation site; green, remaining phosphate groups along the DNA double helix. Tracing the Azo-PM molecule from top to bottom corresponds to the structure from left to right, as depicted in Scheme 2.

Figure 3 shows a phase diagram of the DNA/Azo-PM complex where one can recognize three different ranges: I (black triangles) represents coil-like DNA conformations, while range II (red triangles) displays compacted DNA/Azo-PM complexes. Range III is discussed below. After irradiation with UV light, the DLS intensity distribution of the DNA/Azo-PM complexes changes back to the "fingerprint" shape typical of uncompacted DNA indicating a process of decompaction. The light-driven complete decompaction of the DNA/Azo-PM complex can be achieved only up to some maximum Z values as designated by the gray area (region II) in the phase diagram (Figure 3). At larger concentrations of Azo-PM (range III in the phase diagram), compaction is found to be irreversible (Figure 4g,h). The compaction/decompaction process can reversibly be triggered by periodic irradiation with UV (decompaction, *trans*–*cis*) and blue light (compaction, *cis*–*trans*) only within range II.

A direct visualization of the reversible light induced DNA/Azo-PM compaction can be provided by the corresponding AFM images (Figure 4). In the absence of the compacting agent, the DNA strands appear as long flexible chains (uncompacted state, see Figure 4a). The elongated coil conformation of the chains does not change at low concentration of Azo-PM, but as its concentration increases a significant change in shape is observed. At $Z = 30$ (Figure 4b), the DNA appears to be in a compacted state involving several folds. "Loop"- or "flower"-like morphologies on mica, as depicted in Figure 4b,c, have previously been reported in compaction studies using multivalent organic cations.[57] Further increase of Azo-PM concentration enhances compaction (Figure 4c,d). At $Z = 60$, the majority of chains are in the compacted state; even under UV-irradiation, the decompaction now seems to be incomplete (Figure 4c,g). At very high Azo-PM concentrations, $Z > 100$, the compaction is irreversible (Figure 4d,h). The conformation of the compacted objects resembles a bow-knot shape, an AFM cross-sectional analysis of which reveals a layered structure (Figure 4e). The bottom layer is represented by segments of DNA chains with a height of 0.5 nm, a value typical of single DNA strands adsorbed on mica. The second layer extends to a height of 1.3 nm, most likely single strands of the DNA adsorbed on top of the bottom layer. The central part represents a compacted state with a height between 4 and 7 nm. Upon UV exposure of compacted DNA in solution, the unfolding takes place during 10 min irradiation as monitored by DLS and AFM (Figure 4f).

Discussion and Computational Results. As has been pointed out in the Introduction, the molecular architecture of Azo-PM is somewhat in between that of simple cationic surfactant such as azo-TAB,[21] CTAB,[58] and that of a multivalent cation such as the familiar spermidine (+3).[59] For simple, monovalent cationic lipids/surfactants, a picture of a two-stage mechanism has been shaped by which initially single surfactant molecules bind to the DNA surface, followed by a highly cooperative process where a DNA–surfactant complex is formed. This process is driven by hydrophobic interactions[60] that should lead to the formation of positively charged micellar aggregates in the vicinity of the double helix at concentrations much lower than the CMC,[61] tying the DNA strand together by conveying, for example, electrostatic attraction, in combination with entropic forces (expulsion of monovalent counterions).[62] The precise morphology of the DNA–surfactant complex and the competition between various types of forces driving compaction should, however, depend sensitively on surfactant structure, as well as on environmental conditions such as ionic strength. In mixtures of cationic- with phospho- lipids in complex with DNA, ordered lamellar phases can be formed[63] or even rather dense smectic arrangements.[64]

With azo-containing surfactant, such as azo-TAB,[21] *trans*–*cis* isomerization tends to disrupt formed aggregates by reducing the hydrophobicity of the tails and, hence, triggering decompaction. Our previous work on DNA compaction employing the surfactant azo-TMAB[33] confers with the above-described complex formation: rather

DOI: 10.1021/acs.biomac.6b00052
Biomacromolecules 2016, 17, 1959–1968

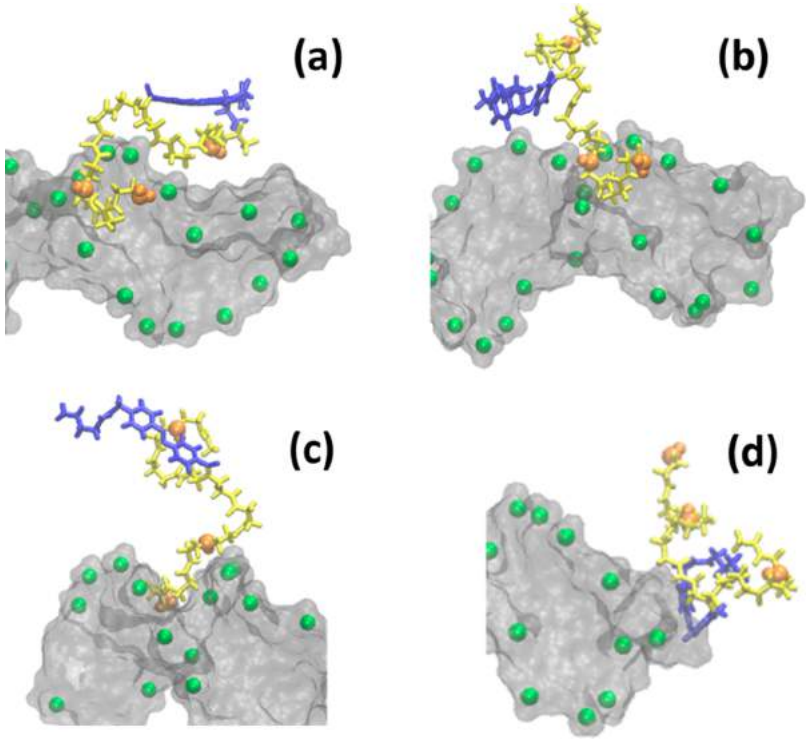

Figure 6. Snapshots of *trans*- and *cis*-Azo-PM in its protonated ((a) and (b), snapshot taken after 200 ns simulation time) and unprotonated ((c) and (d), taken after 80 and 200 ns, respectively) interacting with the DNA double helix. Each snapshot has been rotated around the DNA long axis as to display the Azo-PM most conveniently.

small charge ratios Z are required until single-coil collapse sets in, the transition to the globular state was observed for Z as low as 0.3 (at $C_{Nuc} = 1 \times 10^{-5}$ M).[33] The DNA precipitates out of solution for $1.2 < Z < 2.4$, and for Z larger than 2.4, the globules are positively charged and colloidally stable. The surfactant displays the common structure of a rather small cationic headgroup and a relatively large hydrophobic tail. The behavior should be contrasted to that of Azo-PM, where the complex is still slightly negative for Z as large as 30 (zeta-potential measurements scatter between −15 and −20 mV) and becomes irreversibly compact at sufficiently high Z values (region III in Figure 4). In summary, this points to a qualitatively different route to compaction than with an aggregate forming surfactant.

In the case of Azo-PM, it appears plausible that it should act more as a multivalent cation (such as spermidine). DNA collapse induced by multivalent counterions is also assumed to proceed in two steps: initial single-ion binding events followed by cooperative association preceding collapse. The stabilization of the compacted state is usually attributed to, for example, self-organizing surface lattices, where condensed multivalent ions bridge neighboring DNA strands or charge fluctuations, in the case of mobile multivalent species.[65,66] It is expected that prior to DNA compaction, up to 90% of the bare phosphate charge must be neutralized.[59,67] This would require tight association of Azo-PM's cationic backbone with the DNA surface and at least some of the conformational entropy will be sacrificed.

In the following, we shall therefore shed more light on how Azo-PM behaves in close proximity to the DNA surface with the help of molecular dynamics simulations. We employ the atomistic MM model for Azo-PM described in Experimental Section. Our simulation setup consists of a single surfactant molecule interacting with a straight, double helical DNA segment of 64 Å length, consisting of 20 base pairs (sequence GGCAGTTTGCCTATTTCCTC) with 38 charged phosphate groups, contained in a rectangular simulation box of 102 Å edge length in z, and 65 Å × 65 Å in xy-direction, with periodic boundary conditions imposed. For the fully protonated Azo-PM, charge neutrality is achieved by replacing 35 water molecules with sodium counterions, with no additional salt ion pair (at a salt concentration of 5 mM NaCl, we would on average expect less than one additional ion pair in our simulation box). The size of the simulation box is nevertheless sufficient to capture the local ionic atmosphere around the DNA; note also that at the Azo-PM concentrations used in this work, the presence of the multivalent species in combination with its own counterions (OH^-) does not appreciably affect the Debye length, which evaluates to 4.3 nm in pure 5 mM NaCl solution and 4.06 nm with azo-PM added ($C_{Azo\text{-}PM} = 0.1$ mM) at full protonation. The most important effects should actually be related to condensed counterions, that is, those that determine the effective bare surface charge of the DNA.

The DNA segment was kept in the center of the simulation box parallel to the z-axis by restraints (5000 kJ/mol/nm^2 in x, y, and z directions) of two atoms at the opposing ends of each of the two nucleotide sequences. This restraint is just to facilitate data analysis and does not alter the double helix structure in any way compared to a freely tumbling DNA segment. The duration of a single simulation is 200 ns and should well exceed the time (∼50 ns) expected to arrive at an equilibrated counterion atmosphere.[68] Data were taken every 10 ps, resulting in 20.000 frames for acquiring statistics.

All simulations were started with Azo-PM's oligo(amidoamine) backbone oriented parallel to the DNA, positioned roughly 3 Å apart. The mutual proximity of amine and phosphate groups was analyzed in terms of direct contact, that is, all encounters of any nitrogen closer to a phosphor atom than 4 Å were recorded, corresponding to a VdW contact between the amine and one of the oxygens. Figure 5 shows one Azo-PM (*trans*) attached to the double helix to illustrate this procedure.

Figure 6 shows typical snapshots of each of the Azo-PM configurations (extended sequences are provided in the Supporting Information, Figures S6−S9. Figure 6a and b show the fully protonated surfactant with the azo moiety as *trans*- and *cis*-isomer, respectively. Figure 6c and d show the corresponding situation with the neutral unprotonated surfactant. From the inspection of the MD trajectories, we can infer that fully protonated Azo-PM swiftly approaches the DNA surface and resides there stably for the whole simulation time. The average number of charge−charge contacts is about (2.0 ± 0.1) for the *trans*-isomer and (1.5 ± 0.1) for the *cis*-

DOI: 10.1021/acs.biomac.6b00052
Biomacromolecules 2016, 17, 1959−1968

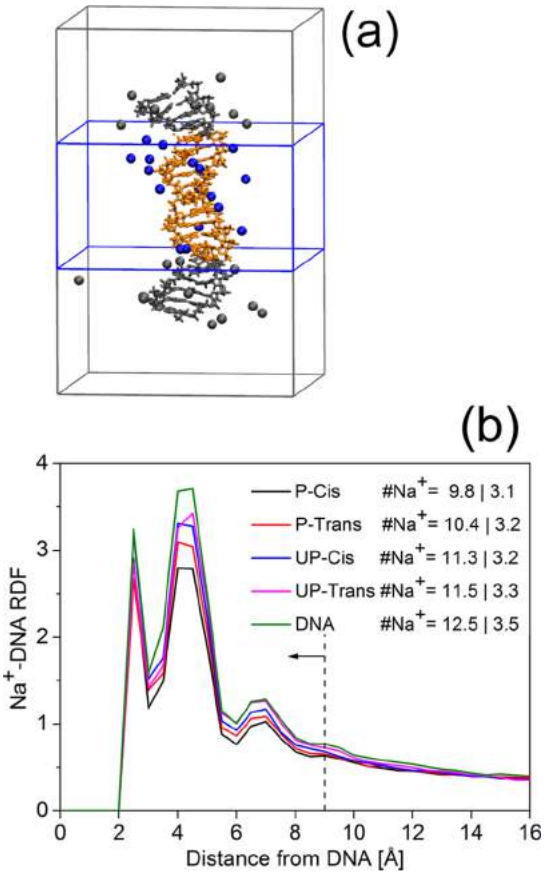

Figure 7. Distribution of counterions around the DNA phosphate groups. (a) Schematic representation of the setup used to estimate the counterion distribution. Spheres: sodium counter ions; for the snapshot shown, the ones kept in blue contribute to the statistics. (b) Na^+ distribution function for the protonated (P)/unprotonated (UP) Azo-PM with the azo-moiety in its *cis* and *trans* state, respectively. The dashed line at 9 Å away from the phosphate groups marks the approximate location of the expected Manning radius,[68] and the inset summarizes how many of the counterions are found on average within the Manning core region (left number) and outside of it (right number). Errors in ion number are about 0.1. Note the unexpected difference between protonated *cis* (black curve, P-Cis in legend) and *trans* (red curve, P-trans in legend), which can be explained by a statistical artifact: in the case of P-trans, actually only 2.19 of all three amine groups are within the central slab for all 20000 frames (the statistics for Na^+ is restricted to this region), compared to 2.45 in the case of P-Cis.

isomer. In both cases, the largest contribution comes from sites 1 and 2 (see Scheme 2), which are ∼1.4 nm apart and predominantly bridge two phosphate groups across the minor groove of the DNA, whereas site 3 and the rest of the Azo-PM molecule are rather flexible. In only 7.2% (24.0%) of all frames were all three protonation sites found in direct contact to DNA phosphates in case of the cis (trans) isomer. The statistical preference for the combination of sites 1 and 2 might naturally be understood as resulting from an enhanced multivalency effect: the shorter segment between 1 and 2 is stiffer, and less entropic costs for conformational restraints must be afforded than for the segment between sites 2 and 3.

In addition, the whole molecule migrates roughly a few nucleotides along the DNA within ∼100 ns; although it maintains its association with the minor groove phosphates, there is no unique binding pose. For comparison, we have considered the molecule in its neutral, unprotonated state (affording three additional Na^+ counterions), see Figure 6c and d, for the *trans*- and *cis*-configuration, respectively.

In contrast to the protonated species, the neutral molecule shows no immediate affinity toward the DNA and first retreats from the double helix by simple diffusive motion. The snapshot in (c) shows an association of Azo-PM with the minor groove. This (temporary) binding pose is found in the corresponding simulation only after 80 ns; during the remaining time the molecule keeps close contact to the double helix, but changes its pose continuously. The number of direct phosphate-amine contacts as defined above is found to be close to zero. The *cis*-isomer is not observed to associate with the DNA surface at all; at the end of each simulation run, it is found trapped at either *end* of the DNA segment.

Note that the situation of completely deprotonated Azo-PM is rather unlikely (see the note on the protonation state of polyamines in Experimental Results), but it allows us to extrapolate toward situations where the protonation may change, for example, due to a drastic change in local dielectric permittivity. Any partial deprotonation would decrease the affinity of Azo-PM toward the DNA, and would increasingly emphasize differences between *cis*- and *trans*-isomerization. It is more difficult to predict, however, if and to what extent the protonation state is affected. For the simulation, this would require the use of all-atom MD with titratable sites.[69] However, application and testing of this technique for the case of DNA complexation would constitute of study of its own.

We have just seen that two of the three amine groups (under full protonation) attach directly to two phosphates, while the third one is dangling. It is instructive to characterize the ion atmosphere around the DNA strand in the presence of the protonated Azo-PM, using a setup as shown in Figure 7a. In order to reduce end effects we restrict the analysis to a central slab (blue solid frame in Figure 7a) of the simulation box, hosting a reference segment consisting of 10 base pairs, where the protonated Azo-PM is found in this region for most of the simulation time. We determined the average number $n(r)$ of Na^+ counterions within a given distance r from the phosphates of the reference segment. A counterion within the central slab contributes to $n(r)$ if any of the reference phosphates is contained within a sphere of radius r around it (in this way, also Na^+ ions penetrating into the grooves are recorded). Differentiating $n(r)$, we obtain the density distributions displayed in Figure 7b, which are quite similar to those obtained by Savelyev and Papoian in their study of the condensation of monovalent counter ions to neutralize the bare DNA phosphate charges[68] (Papoian and Savelyev determine the actual radial distribution function $g(r)$, which is related to $n(r)$ through $n(r) = \rho J(r) g(r)$ where J denotes the volume Jacobian, determined by careful numerical analysis, and ρ denotes the bulk ionic density. We do not need this degree of detail for the present discussion). The density peaks at ∼ 3Å, 5Å and 7Å indicate the layering of the condensed, or "tightly bound" portion of Na^+ ions, which are expected to neutralize roughly 76% of the phosphate groups[70] (and define the effective DNA surface charge), followed by a diffuse Debye-Hückel layer of "free" counter ions. We find that this separation occurs at ∼9 Å consistent with Savelyev's study.[68] In addition to the simulation runs with protonated and unprotonated Azo-PM in its *cis*- and *trans*-state, respectively, a run without it was performed (green line). We learn immediately in going from protonated to unprotonated Azo-PM and finally to the clean run, that the Azo-PM approximately replaces three sodium ions in the condensed layer.

As the diffuse region is essentially left unaffected, these ions can be considered as set free with a corresponding gain in translational entropy. We should note, however, that the current simulation setup is not geared toward quantifying entropic gains/losses upon release of monovalent counterions/conformational restraints of the multivalent ligand. Such questions require coarser levels of description[71] and are also not essential to typical mean-field theories of single coil collapse: the fraction of released monovalent counterions is treated as an adjustable parameter.[62] However, given the stable association of the protonated Azo-PM with the DNA surface just described, we should rather like to ask how Azo-PM can tune the process of compaction. A primary role as a multivalent cation would naturally explain the existence of the irreversible region III: above a certain Z-value, only the amount of cation content in the vicinity of the DNA strand governs

DOI: 10.1021/acs.biomac.6b00052
Biomacromolecules 2016, 17, 1959−1968

the transition to the collapsed state, independent of the isomerization state of the azobenzene moiety. Below a critical *Z*-value, *trans*−*cis* isomerization can then be expected to modulate this behavior. On the one hand, Azo-PM molecules in their *trans* state would render the DNA strand effectively more hydrophobic and support the stabilization of a compact state, even at comparably low cation concentration, by cooperatively forming nucleation centers, leading to the flower-like aggregates apparent from Figure 4. On the other, the isomerization state could also regulate the very amount of adsorbed Azo-PM. From the MD simulations we obtain indications that the association of the molecule with DNA in *trans* is tighter than in the *cis* state.

The scenarios described above should still be accessible to large scale all-atom MD simulation involving, say, two opposing DNA strands of 100 bp each, 100 Azo-PM under varying salt conditions. Furthermore, it should be possible to obtain further evidence on whether aggregates of Azo-PM may form at all, a mechanism that for now has indirectly been excluded. These questions are currently under investigation and will be published in future work.

Summary. We report on a new, efficient peptidomimetic, photosensitive compacting agent (Azo-PM) for reversible DNA compaction. Azo-PM was synthesized using a solid-phase procedure, its photosensitive azo-moiety bears stable *trans*- and *cis*-isomers, and fast light-induced switching between both states. The addition of Azo-PM to DNA above certain concentrations results in DNA compaction. We could verify the existence of the compacted state by dynamic light scattering (DLS) and atomic force microscopy (AFM), where compacted DNA could be studied on mica surfaces, suggesting that the compacted state consists of dense nuclei connected by extended loops. Depending on the concentration of Azo-PM, three distinct phases could be identified, with DNA in a (i) coil-like, noncompacted state, (ii) compacted reversible state, and (iii) compacted irreversible state. Only complexes from the reversible phase can be decompacted by an optical stimulus alone. The ratio of DNA phosphate to Azo-PM charge required to achieve compaction suggests that Azo-PM leads to a different route of compaction than familiar compacting agents, such as CTAB, Azo-TAB, or C_4-AzoOC_6-TMAB. Results from molecular dynamics simulations sustain the interpretation that Azo-PM could act primarily as a multivalent cation, the compaction efficiency of which is modulated by the presence of the azo-moiety. Our study shows that photosensitive azo-moieties may successfully employed as part of compacting agents that do not share a conventional surfactant structure, but contain cationic elements that eventually lead to nontoxic photosensitive vectors for gene delivery.

■ ASSOCIATED CONTENT

Supporting Information

The Supporting Information is available free of charge on the ACS Publications website at DOI: 10.1021/acs.biomac.6b00052.

The ^{1}H NMR, RP-HPLC, and ESI-MS data of the final product are presented in Figures S1−S3. The analysis of the lifetime of the *cis*-isomer is shown in Figure S4. DLS data for different *Z* values are presented in Figure S5. Extended sequences of typical snapshots of each of the Azo-PM configurations are provided in Figures S6−S9 (PDF).

■ AUTHOR INFORMATION

Corresponding Authors

*E-mail: santer@uni-potsdam.de.
*E-mail: mark.santer@mpikg.mpg.de.
*E-mail: laura.hartmann@hhu.de.

Present Address

[‖]Institute of Organic Chemistry and Macromolecular Chemistry, Heinrich-Heine-Universität, 40225 Duesseldorf, Germany.

Notes

The authors declare no competing financial interest.

■ ACKNOWLEDGMENTS

This research is supported by the International Max Planck Research School on Multiscale Bio-Systems (IMPRS), Potsdam, Germany. N.M.M.-N. and L.H. would like to thank the Boehringer Ingelheim Foundation for financial support through the PLUS 3 program.

■ REFERENCES

(1) Vijayanathan, V.; Thomas, T.; Thomas, T. J. *Biochemistry* **2002**, *41*, 14085−14094.
(2) Demeneix, B.; Hassani, Z.; Behr, J. *Curr. Gene Ther.* **2004**, *4*, 445−455.
(3) Estévez-Torres, A.; Baigl, D. *Soft Matter* **2011**, *7*, 6746−6756.
(4) Richards, E. J.; Elgin, S. C. R. *Cell* **2002**, *108*, 489−500.
(5) Browning, D. F.; Busby, S. J. *Nat. Rev. Microbiol.* **2004**, *2*, 57−65.
(6) Dillon, S. C.; Dorman, C. J. *Nat. Rev. Microbiol.* **2010**, *8*, 185−195.
(7) Cerritelli, M. E.; Cheng, N.; Rosenberg, H.; McPherson, C. E.; Booy, F. P.; Steven, C. *Cell* **1997**, *91*, 271−280.
(8) Montier, T.; Benvegnu, T.; Jaffrès, P.-A.; Yaouanc, J.-J.; Lehn, P. *Curr. Gene Ther.* **2008**, *8*, 296−312.
(9) Bloomfield, V. A. *Biopolymers* **1997**, *44*, 269−282.
(10) Li, Y.; Yildiz, U. H.; Muellen, K.; Grohn, F. *Biomacromolecules* **2009**, *10*, 530−540.
(11) Wang, X.-L.; Zhang, X.-H.; Cao, M.; Zheng, H.-Z.; Xiao, B.; Wang, Y.; Li, M.; Gemini. *J. Phys. Chem. B* **2009**, *113*, 2328−2332.
(12) Leforestier, A.; Livolant, F. *Proc. Natl. Acad. Sci. U. S. A.* **2009**, *106*, 9157−9162.
(13) van den Broek, B.; Noom, M. C.; van Mameren, J.; Battle, Ch.; MacKintosh, F. C.; Wuite, G. J. L. *Biophys. J.* **2010**, *98*, 1902−1910.
(14) Carnerup, A. M.; Ainalem, M.-L.; Alfredsson, V.; Nylander, T. *Langmuir* **2009**, *25* (21), 12466−12470.
(15) Golan, R.; Pietrasanta, L. I.; Hsieh, W.; Hansma, H. G. *Biochemistry* **1999**, *38*, 14069−14076.
(16) Osada, K.; Oshima, H.; Kobayashi, D.; Doi, M.; Enoki, M.; Yamasaki, Y.; Kataoka, K. *J. Am. Chem. Soc.* **2010**, *132*, 12343−12348.
(17) Hartmann, L.; Häfele, S.; Peschka-Süss, R.; Antonietti, M.; Börner, H. G. *Chem. - Eur. J.* **2008**, *14*, 2025−33.
(18) Wagner, E. *Adv. Genet.* **2014**, *88*, 231−61.
(19) Rudiuk, S.; Venancio-Marques, A.; Baigl, D. *Angew. Chem., Int. Ed.* **2012**, *51*, 12694−12698.
(20) Cinque, L.; Ghomchi, Y.; Chen, Y.; Bensimon, A.; Baigl, D. *ChemBioChem* **2010**, *11*, 340−343.
(21) Le Ny, A.-L.; Lee, C. *J. Am. Chem. Soc.* **2006**, *128*, 6400−6408.
(22) Le Ny, A.-L.; Lee, C. *Biophys. Chem.* **2009**, *142*, 76−83.
(23) Rau, H. Photoisomerization of azobenzenes. In *Photochemistry and Photophysics*; Rabeck, J. F., Eds.; CRC: Boca Raton, FL, 1990; Vol *II*, pp 119−142.
(24) Zakrevskyy, Y.; Richter, M.; Zakrevska, S.; Lomadze, N.; von Klitzing, R.; Santer, S. *Adv. Funct. Mater.* **2012**, *22*, 5000−5009.
(25) Sollogoub, M.; Guieu, S.; Geoffroy, M.; Yamada, A.; Estévez-Torres, A.; Yoshikawa, K.; Baigl, D. *ChemBioChem* **2008**, *9*, 1201−1206.
(26) Geoffroy, M.; Faure, D.; Oda, R.; Bassani, D.; Baigl, D. *ChemBioChem* **2008**, *9*, 2382−2385.
(27) Diguet, A.; Mani, N.; Geoffroy, M.; Sollogoub, M.; Baigl, D. *Chem. - Eur. J.* **2010**, *16*, 11890−11896.
(28) Rudiuk, S.; Yoshikawa, K.; Baigl, D. *Soft Matter* **2011**, *7*, 5854−5860.

DOI: 10.1021/acs.biomac.6b00052
Biomacromolecules 2016, 17, 1959−1968

(29) Zinchenko, A.; Tanahashi, M.; Murata, S. *ChemBioChem* **2012**, *13*, 105−111.
(30) Zakrevskyy, Y.; Kopyshev, A.; Lomadze, N.; Morozova, E.; Lysyakova, L.; Kasyanenko, N.; Santer, S. *Phys. Rev. E* **2011**, *84*, 021909.
(31) Zakrevskyy, Y.; Cywinski, P.; Cywinska, M.; Paasche, J.; Lomadze, N.; Reich, O.; Löhmannsröben, H.-G.; Santer, S. *J. Chem. Phys.* **2014**, *140*, 044907.
(32) Zakrevskyy, Y.; Roxlau, J.; Brezesinski, G.; Lomadze, N.; Santer, S. *J. Chem. Phys.* **2014**, *140*, 044906.
(33) Zakrevskyy, Yu.; Titov, E.; Lomadze, N.; Santer, S. *J. Chem. Phys.* **2014**, *141*, 164904.
(34) Scholz, C.; Kos, P.; Leclercq, L.; Jin, X.; Cottet, H.; Wagner, E. *ChemMedChem* **2014**, *9*, 2104−10.
(35) Wojcik, F.; Mosca, S.; Hartmann, L. *J. Org. Chem.* **2012**, *77* (9), 4226−4234.
(36) Behrendt, R.; Schenk, M.; Musiol, H.-J.; Moroder, L. *J. Pept. Sci.* **1999**, *5*, 519−529.
(37) Rück-Braun, K.; Kempa, S.; Priewisch, B.; Richter, A.; Seedorff, S.; Wallach, L. *Synthesis* **2009**, *24*, 4256−4267.
(38) Ponader, D.; Wojcik, F.; Beceren-Braun, F.; Dernedde, J.; Hartmann, L. *Biomacromolecules* **2012**, *13* (6), 1845−1852.
(39) Gude, M.; Ryf, J.; White, P. D. *Lett. Pept. Sci.* **2002**, *9*, 203.
(40) Frisch, M. J.; Trucks, G. W.; Schlegel, H. B.; Scuseria, G. E.; Robb, M. A.; Cheeseman, J. R.; Montgomery, J. A., Jr.; Vreven, T.; Kudin, K. N.; Burant, J. C.; Millam, J. M.; Iyengar, S. S.; Tomasi, J.; Barone, V.; Mennucci, B.; Cossi, M.; Scalmani, G.; Rega, N.; Petersson, G. A.; Nakatsuji, H.; Hada, M.; Ehara, M.; Toyota, K.; Fukuda, R.; Hasegawa, J.; Ishida, M.; Nakajima, T.; Honda, Y.; Kitao, O.; Nakai, H.; Klene, M.; Li, X.; Knox, J. E.; Hratchian, H. P.; Cross, J. B.; Bakken, V.; Adamo, C.; Jaramillo, J.; Gomperts, R.; Stratmann, R. E.; Yazyev, O.; Austin, A. J.; Cammi, R.; Pomelli, C.; Ochterski, J. W.; Ayala, P. Y.; Morokuma, K.; Voth, G. A.; Salvador, P.; Dannenberg, J. J.; Zakrzewski, V. G.; Dapprich, S.; Daniels, A. D.; Strain, M. C.; Farkas, O.; Malick, D. K.; Rabuck, A. D.; Raghavachari, K.; Foresman, J. B.; Ortiz, J. V.; Cui, Q.; Baboul, A. G.; Clifford, S.; Cioslowski, J.; Stefanov, B. B.; Liu, G.; Liashenko, A.; Piskorz, P.; Komaromi, I.; Martin, R. L.; Fox, D. J.; Keith, T.; M. A., Al-Laham, Peng, C. Y.; Nanayakkara, A.; Challacombe, M.; Gill, P. M. W.; Johnson, B.; Chen, W.; Wong, M. W.; Gonzalez, C.; Pople, J. A. *Gaussian 03*, Revision E.01.; Gaussian, Inc., Wallingford, CT, 2004.
(41) Case, D. A.; Babin, V.; Berryman, J. T.; Betz, R. M.; Cai, Q.; Cerutti, D. S.; Cheatham, T. E., III; Darden, T. A.; Duke, R. E.; Gohlke, H.; Goetz, A. W.; Gusarov, S.; Homeyer, N.; Janowski, P.; Kaus, J.; Kolossváry, I.; Kovalenko, A.; Lee, T. S.; LeGrand, S.; Luchko, T.; Luo, R.; Madej, B.; Merz, K. M.; Paesani, F.; Roe, D. R.; Roitberg, A.; Sagui, C.; Salomon-Ferrer, R.; Seabra, G.; Simmerling, C. L.; Smith, W.; Swails, J.; Walker, R. C.; Wang, J.; Wolf, R. M.; Wu, X.; Kollman, P. A. *AMBER 14*; University of California, San Francisco, CA, 2014.
(42) Hornak, V.; Abel, R.; Okur, A.; Strockbine, B.; Roitberg, A.; Simmerling, C. *Proteins: Struct., Funct., Genet.* **2006**, *65*, 712−725.
(43) Wang, J.; Wolf, R. M.; Caldwell, J. W.; Kollman, P. A.; Case, D. A. *J. Comput. Chem.* **2004**, *25*, 1157−1174.
(44) Duchstein, P.; Neiss, C.; Görling, A.; Zahn, D. *J. Mol. Model.* **2012**, *18*, 2479−2482.
(45) Basma, M.; Sundara, S.; Calgan, D.; Vernali, T.; Woods, R. J. *J. Comput. Chem.* **2001**, *22*, 1125−1137.
(46) Jakalian, A.; Jack, D. B.; Bayly, Ch. I. *J. Comput. Chem.* **2002**, *23*, 1623−1641.
(47) Hess, B.; Kutzner, C.; Van Der Spoel, D.; Lindahl, E. GROMACS 4. *J. Chem. Theory Comput.* **2008**, *4*, 435−447.
(48) Wehle, M.; Vilotijevic, I.; Varón Silva, D.; Seeberger, P. H.; Lipowsky, R.; Santer, M. *J. Am. Chem. Soc.* **2012**, *134*, 18964−18972.
(49) Ponader, D.; Igde, S.; Wehle, M.; Märker, K.; Santer, M.; Bléger, D.; Hartmann, L. *Beilstein J. Org. Chem.* **2014**, *10*, 1603−1612.
(50) De Stefano, C.; Giuffrè, O.; Sammartano, S. *J. Chem. Eng. Data* **2005**, *50*, 1917−1923.
(51) Korolev, N.; Lyubartsev, A. P.; Laaksonen, A.; Nordenskiöld, L. *Nucl. Acids. Res.* **2003**, *31*, 5971−5981.
(52) Avogadro: an open-source molecular builder and visualization tool. Version 1.1.1., http://avogadro.openmolecules.net/: Hanwell, M. D.; Curtis, D. E.; Lonie, D. C.; Vandermeersch, Z. E.; Hutchison, G. R.; Zurek, E. Avogadro: An advanced semantic chemical editor, visualization, and analysis platform. *J. Cheminf.* **2012**, *4*, 17.
(53) Marvin (MarvinSketch) was used for drawing, displaying and characterizing chemical structures, substructures and reactions: *Marvin 6.1.3*; ChemAxon, 2013 (http://www.chemaxon.com; https://www.chemaxon.com/forum/ftopic977.html).
(54) Sorlie, S.; Pecora, R. *Macromolecules* **1990**, *23*, 487−497.
(55) Cardenas, M.; Schillen, K.; Nylander, T.; Jansson, J.; Lindman, B. *Phys. Chem. Chem. Phys.* **2004**, *6*, 1603−1607.
(56) Marchetti, S.; Onori, G.; Cametti, C. *J. Phys. Chem. B* **2005**, *109*, 3676−3680.
(57) Li, Y.; Yildiz, U. H.; Müllen, K.; Gröhn, F. *Biomacromolecules* **2009**, *10*, 530−540.
(58) Melnikov, S. M.; Sergeyev, V. G.; Yoshikawa, K. *J. Am. Chem. Soc.* **1995**, *117*, 2401−2408.
(59) Matulis, D.; Rouzina, I.; Bloomfield, V. A. *J. Am. Chem. Soc.* **2002**, *124*, 7331−7342.
(60) Spink, C. H.; Chaires, J. B. *J. Am. Chem. Soc.* **1997**, *119*, 10920−10928.
(61) Santhiya, D.; Dias, R. S.; Dutta, S.; Das, P. K.; Miguel, M. G.; Lindman, B.; Maiti, S. *J. Phys. Chem. B* **2012**, *116*, 5831−5837.
(62) Takahashi, M.; Yoshikawa, K.; Vasilevskaya, V. V.; Khokhlov, A. R. *J. Phys. Chem. B* **1997**, *101*, 9396−9401.
(63) Rädler, J. O.; Kotover, I.; Salditt, T.; Safinya, C. R. *Science* **1997**, *275*, 810−814.
(64) Farago, O.; Gronbech-Jensen, N. *J. Am. Chem. Soc.* **2009**, *131*, 2875−2881.
(65) Matulis, D.; Rouzina, I.; Bloomfield, V. A. *J. Mol. Biol.* **2000**, *296*, 1053−1063.
(66) Naji, A.; Arnold, A.; Holm, C.; Netz, R. R. *Europhys. Lett.* **2004**, *67*, 130−136.
(67) Widom, J.; Baldwin, R. L. *Biopolymers* **1983**, *22*, 1595−1620.
(68) Savelyev, A.; Papoian, G. A. *J. Am. Chem. Soc.* **2006**, *128*, 14506−14518.
(69) Wallace, J. A.; Shen, J. K. J. *J. Chem. Phys.* **2012**, *137*, 184105.
(70) Manning, G. S. *Acc. Chem. Res.* **1979**, *12*, 443−449.
(71) Stevens, M. J. *Biophys. J.* **2001**, *80*, 130−139.

DOI: 10.1021/acs.biomac.6b00052
Biomacromolecules 2016, 17, 1959−1968